Supplementary information

Table S1. Experimental conditions applied for the potentiometric titrations.

System	phen-H^+	phen-Cu(II)	InsP_6-phen	InsP_6-phen-Cu(II)
Component	Concentration range (mM)			
Cu(II)	---	1.3	---	1.3 – 5.1
InsP_6	---	---	1.3 – 1.8	0.3 – 1.4
phen	1.1 – 2.0	1.4 – 3.8	1.3 – 3.7	1.0 – 4.1
Component ratio	Molar ratio			
InsP_6/Cu(II)	---	---	---	0.3 – 1.0
phen/Cu(II)	---	1.0 – 2.9	---	0.5 – 1.1
InsP_6/phen	---	---	0.3 – 1.0	0.3 – 1.0
Number of titrations	4	4	6	8

Table S2. Crystal data and structure refinement for a) $(Hphen)_4(H_8L)\cdot 6H_2O$ (**1**), and b) $[Cu_5(H_7L)_2(H_2O)_2(phen)_5]\cdot 7.5H_2O$ (**2**).

	(a)	(b)
Empirical formula	$C_{54}H_{63.6}N_8O_{30.8}P_6$	$C_{72}H_{85}Cu_5N_{10}O_{57.5}P_{12}$
Formula weight	1503.34	2699.83
Temperature (K)	120	150
space group	*P-1*	*P 1*
a (Å)	11.299(1)	12.964(1)
b (Å)	11.487(1)	15.316(1)
c (Å)	13.711(2)	15.8016(8)
α (°)	83.501(9)	65.840(6)
β (°)	65.75(1)	87.478(5)
γ (°)	73.380(9)	71.397(5)
Volume ($Å^3$)	1554.7(3)	2699.5(3)
Z	1	1
Independent reflections / R(int)	4461/0.0995	10146/0.0426
μ (mm^{-1}, Cu-Kα)	2.504	3.691
R indices [I>2σ(I)]*	R1 = 0.0758	R1 = 0.1204
	wR2 = 0.1719	wR2 = 0.1850
R indices (all data)*	R1 = 0.1415	R1 = 0.2882
	wR2 = 0.2063	wR2 = 0.3609

* $R1 = \Sigma \, || Fo| - |Fc|| \, / \, \Sigma \, |Fo|$; $wR2 = [\, \Sigma \, w(Fo^2 - Fc^2)^2 \, / \, \Sigma \, wFo^4]^{1/2}$

X-ray diffraction studies

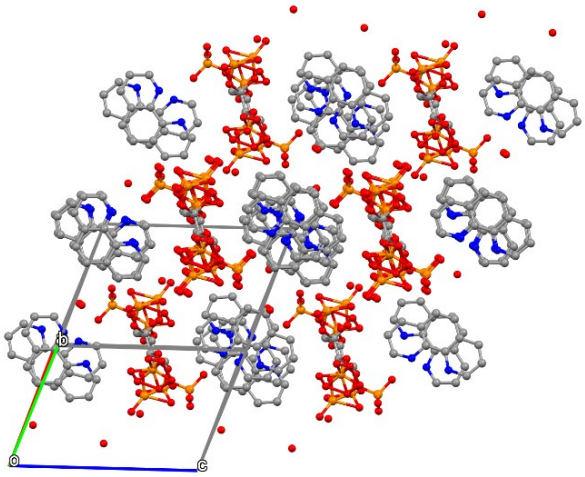

Figure S1. Crystal packing of compound **1**. Color code: C (grey), O (red), N (blue), P (orange). Hydrogen atoms are omitted for clarity.

Infrared spectra

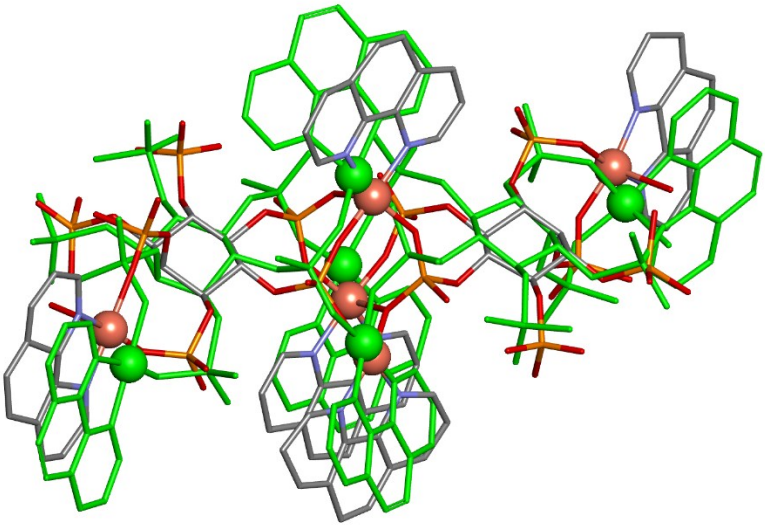

Figure S2. Crystal structure of compound **2**. Color code: C (grey), O (red), N (blue), P (orange), Cu (pink). The DFT optimized geometry in solution for the pentanuclear complex $[Cu_5(H_7L)_2(H_2O)_2(phen)_5]$ is shown superimposed in green. Hydrogen atoms and non-coordinated water molecules are omitted for clarity.

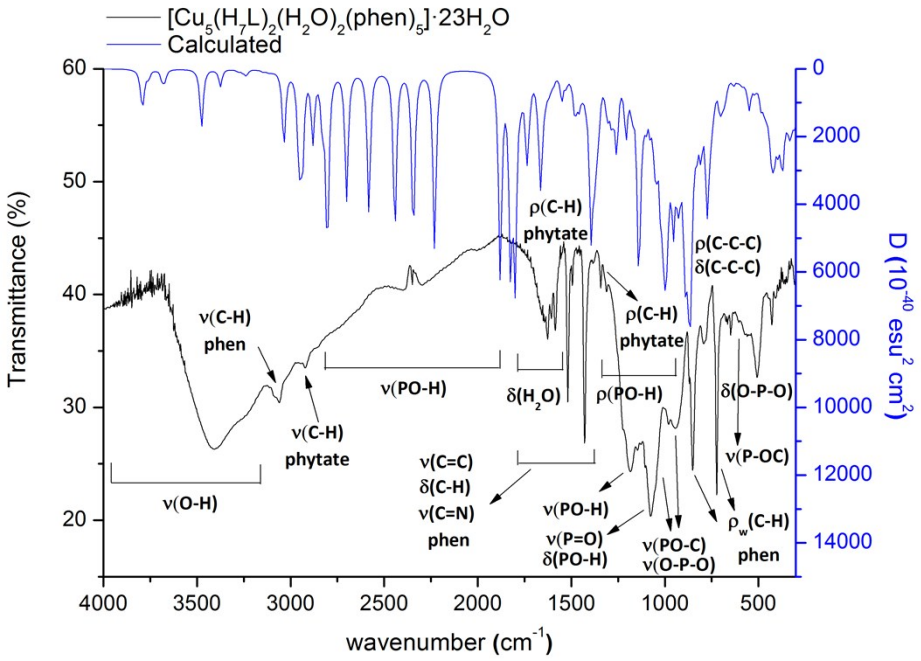

Figure S3. Experimental and calculated (UB3LYP/LANL2DZ) vibrational spectra of compound **2**. The assignation of the associated normal modes is also shown.

Non-isothermal decomposition mechanism and kinetics

The kinetics and rate-dependent parameters of the solid state non-isothermal decomposition reactions were studied using the integral methods of Coats and Redfern (CR)[1] and Horowitz and Metzger (HM),[2] which are the most commonly applied.[3-5] Using both methods, the observed degree of decomposition (α) at various temperatures corresponding to each of the steps in the TG curves were fitted and plotted against a function of temperature for various assumed values of n (reaction order). The most appropriate n value, corresponding to the best straight line (higher correlation coefficient, *r*), and the respective slope was employed to estimate the activation energy of the selected decomposition step (E_a). This kinetic parameter depends on the strength of bonding of water molecules, ligands and counterions. However, due to the existence of various steps involving the loss of more than one group, the calculated E_a is an average value for the overall process. In any case, identical reaction orders and similar values of E_a were obtained for both CR and HM methods for all the decomposition steps under analysis (see Table S3).

The thermal decomposition pathway of **2** involves seven stages (Figure S4). The first step is related to a third-order reaction in which 15 moles of H_2O per mole of complex are released. The second and third steps are associated with the loss of 3 and 5 moles of water molecules, respectively, which are more strongly bound. The more the number of water molecules involved in the process, the higher the activation energy of the dehydration steps (E_a) is. The dehydrated complex is stable up to 250 °C. The fourth step (246 – 300 °C) can be attributed to the partial carbonization and dehydration processes due to the decomposition of 6 -OH groups present in the protonated phytate anion.[6] Along with that, the complex undergoes a dehydration reaction involving the two water molecules still bound to the external copper centers. The overall process has a weight loss of 4.7 % and occurs through a

second-order kinetics with an activation barrier of more than 400 kJ/mol. The partial degradation of phenanthroline starts at about 300 °C, in a first-order reaction involving the concomitant decomposition of an -OH group (E_a ≈ 350 – 380 kJ/mol). According to previous works on copper-phen complexes, the phen moiety can be lost between 160 and 600 °C, and it is sometimes accompanied by the removal of coordinated –OH and H_2O fragments.[7,8] Above 500 °C, the carbonization of **2** becomes evident.

Table S3. TGA data and non-isothermal decomposition kinetics and mechanism parameters for compound **2**. The same data for compound **1**, phenanthroline and the phytate dipotassium salt are also listed.

Solid phase	Temp. range (°C)	% wt. loss exp. (calc.)	Probable composition of expelled group/s	E_a (kJ/mol)[a]		Mechanism[b]
				CR	HM	
$[Cu_5(H_7L)_2(H_2O)_2(phen)_5]\cdot 23H_2O$ (**2**)	22-40	9.2 (9.1)	15 H_2O	570 (3)	569 (3)	F_2
	40-59	1.7 (1.8)	3 H_2O	225 (2)	231 (2)	F_2
	59-100	3.1 (3.0)	5 H_2O	248 (3)	247 (3)	F_2
	246-300	4.7 (4.8)	2 H_2O + 6 OH[c]	422 (2)	414 (2)	A_3
	300-360	9.9 (9.7)	1.5 phen + OH[c]	355 (1)	377 (1)	A_3
	360-500	5.9 (6.0)	1 phen	---	---	---
	500-700	7.2	carbonization	---	---	---
$(Hphen)_4(H_8L)\cdot 7.5H_2O$ (**1**)	24-150	9.0 (8.9)	7.5 H_2O	130 (3)	132 (3)	F_2
	150-350	31.1 (30.9)	2 phen + 6 OH[c]	102 (2)	101 (2)	A_3
	350-700	16.2 (16.6)	1 phen + 4 OH[c]	---	---	---
$K_2H_{10}L\cdot 2.5H_2O$	19-200	5.4 (5.8)	2.5 H_2O	31 (1)	39 (1)	A_3
	200-350	11.8 (11.5)	5 OH[c]	143 (2)	149 (2)	A_3
phenanthroline	25-150	9.4	water desorption and dehydration	---	---	---
	150-250	89.6	decomposition	89 (0)	94 (0)	D_2

[a] E_a refers to per mole of the compound decomposed. CR: Coats and Redfern method.[1] HM: Horowitz and Metzger method.[2] The order of reaction is given between brackets. [b] A3: Avrami-Erofeyev nucleation mechanism for n = 3; D2: two-dimensional diffusion (cylindrical symmetry); F2: random nucleation (second order). [c] OH: partial carbonization and dehydration process of phytate due to the decomposition of the –OH groups.

According to Figure S4, the TG profile for compound **1** shows three different thermal degradation steps. The first stage is associated with a 9.0 % mass loss, corresponding to the release of 7.5 moles of lattice water molecules per mole of compound. This process has a lower activation energy barrier per mole of expelled water molecules in comparison to the dehydration steps of **2**, indicating the presence of weaker water-adduct bonds in the structure of **1**. The next weight loss is observed between 150 and 350 °C (n = 2, E_a ≈ 100 kJ/mol), and involves the decomposition of 2 phen

molecules and 6 -OH groups of phytate, in agreement with the temperature range in which decomposition occurs for phytate ($K_2H_{10}L$) and phen samples. An equivalent thermal process is also detected for compound **2** (fifth step), but even though less moles of phen and –OH groups are decomposed, the activation barrier is even higher due to the stabilization exerted by the copper complexation. Additionally, the interaction of phen and phytate is likely to decrease the non-isothermal kinetic stability of **1**, for the E_a value for the second decomposition step is significantly lower than the addition of those estimated for the same stage of both ligands separately.

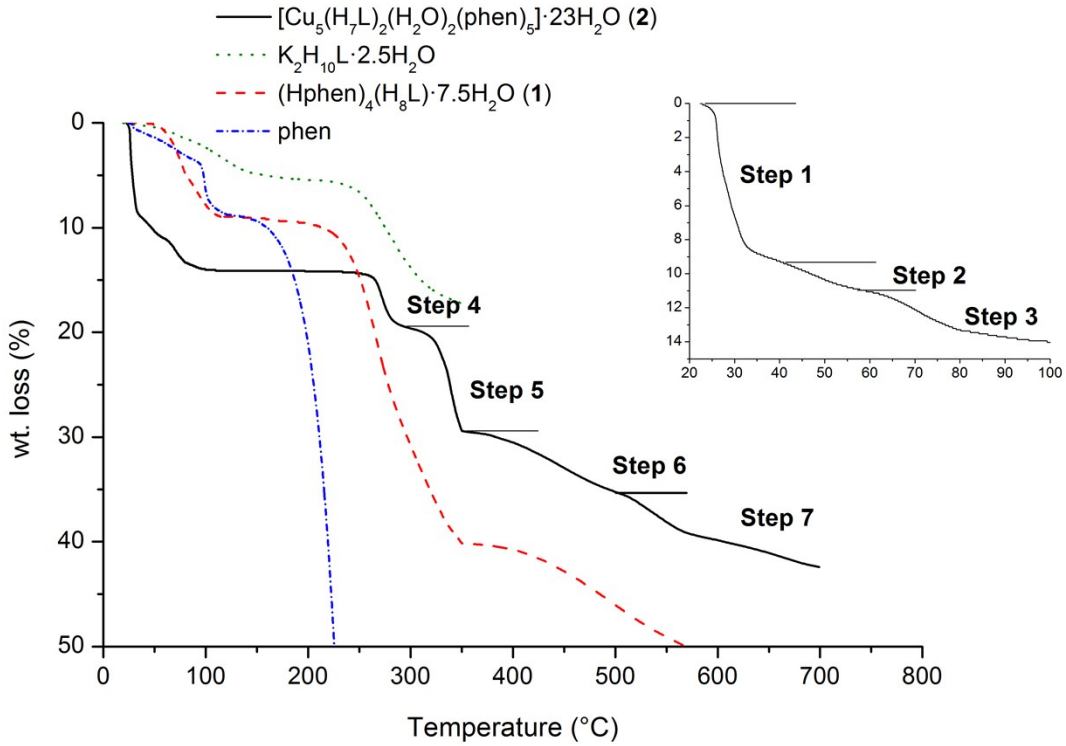

Figure S4. Thermograms of compounds **1**, **2**, phenanthroline and the phytate dipotassium salt. The different thermal decomposition steps of **2** are also depicted. The inset shows a zoom of the TGA curve of **2** in the 20 – 100 °C range.

The α *vs*. temperature data for each step in a TG curve was used to deduce the most probable mechanism underlying the most important decomposition steps of the TG of compounds **1**, **2**, phenanthroline and phytate dipotassium salt (see Figures S5a and b as examples). Many models were tested, by plotting the quantity –log(g(α)) *vs*. 1/*T*, leading to the best linear fit of the non-isothermal α-temperature plots.[9,10] The results are included in Table S3, where the symbols A, D, F, R and their subscripts represent the different mechanistic models.[9]

The dehydration steps of compounds **1** and **2** are found to fit to the random nucleation F_2 model. In this regard, the reaction rate decreases with reaction progress, as the amount of water molecules remaining in the lattice is progressively reduced. This mechanism is not the same for the dehydration of phytate dipotassium salt, which obeys the Avrami-Erofeyev nucleation model for n = 3 (A_3). This model is also the one that describes the mechanistic features of the ligand decomposition steps of all the phytate compounds analyzed (Table S3). This is not unexpected, since many solid-state reactions

have been described by the nuclei growth model. For instance, phen decomposition in $[Cu(phen)_2]Cl_2 \cdot 2H_2O$ fits to the A_2 mechanism.[5] According to the Avrami-Erofeyev model, the solid-state decomposition starts by random nuclei formation, followed by growth under certain restrictions related to ingestion and coalescence processes. When phytate and copper are absent, the mechanistic characteristics change significantly, and phenanthroline decomposes according to a two-dimensional diffusion D_2 mechanism, in which the solid particles are cylindrical and the reaction occurs through radial diffusion.

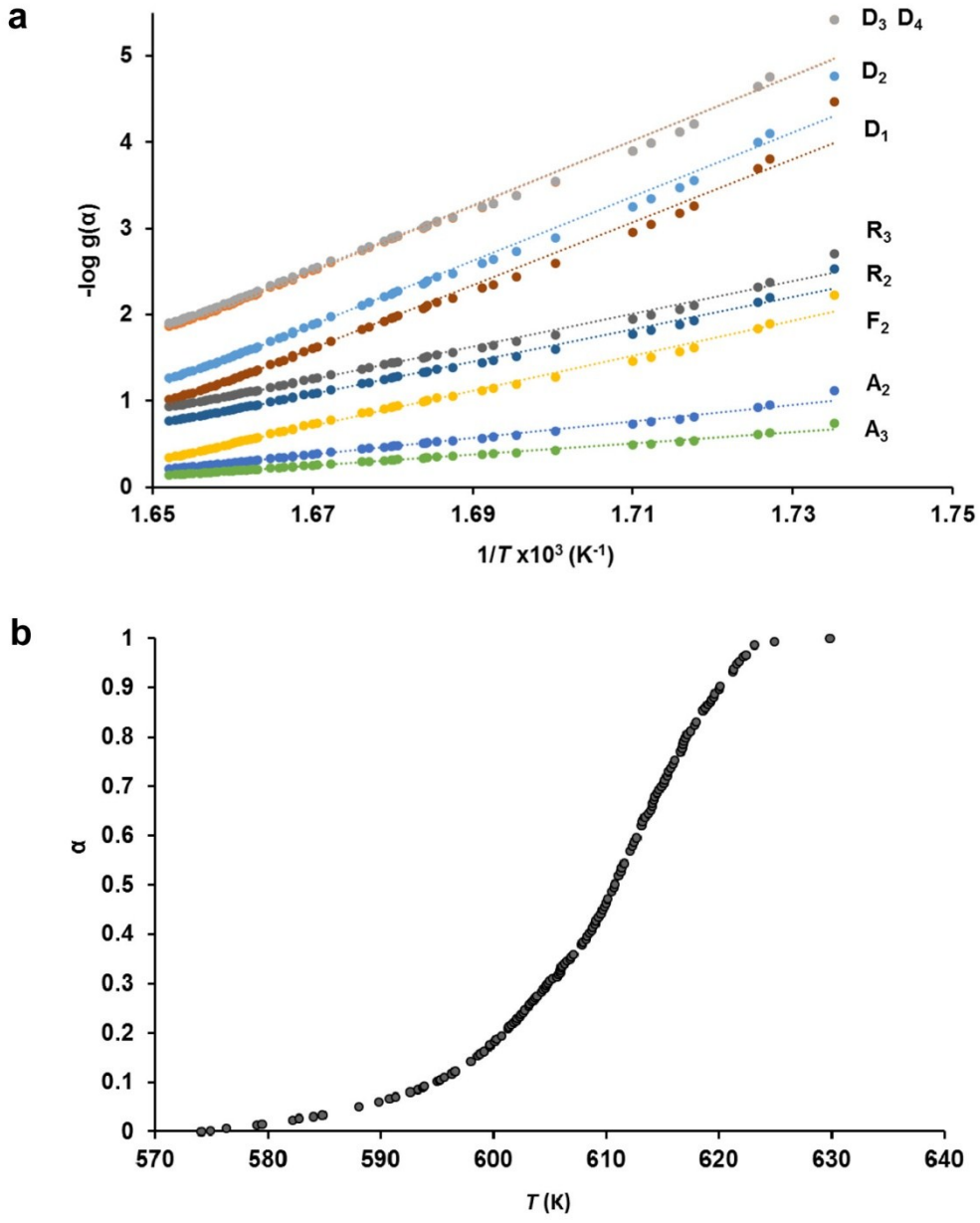

Figure S5. Plots used for determining the most probable reaction mechanism applied to the fifth step of the non-isothermal decomposition of complex **2.** a) -log g(α) *vs.* 1/*T* curve gives the best linear fit for the A_3 mechanism. b) This sigmoidal kinetic model is verified by plotting α as the temperature varies.

Solution studies

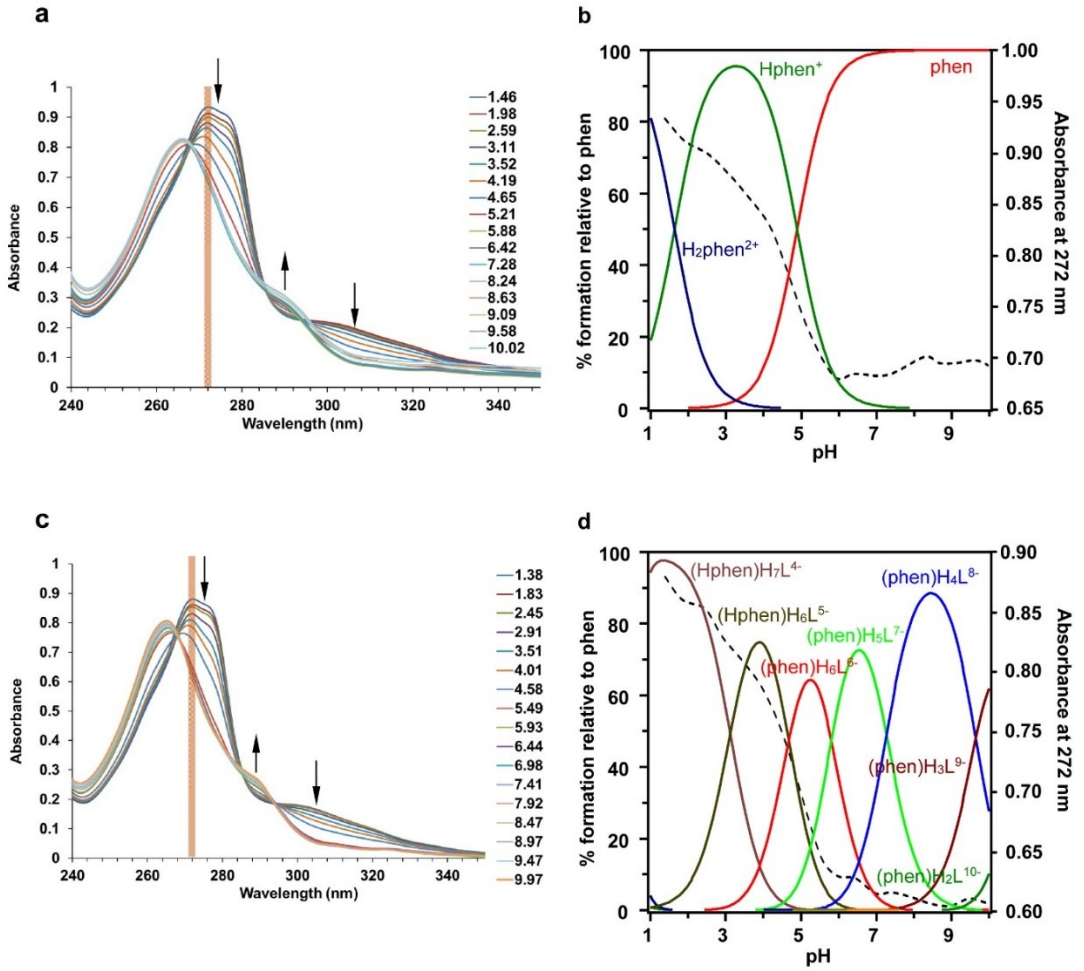

Figure S6. a) UV-vis spectra of phen as the pH varies ([phen] = 0.032 mM, in 0.15 M NMe_4Cl at 27 °C). The absorbance at 272 nm is highlighted. b) Species distribution for phen under similar conditions at 37.0 °C. The variation of the absorbance at 272 nm with pH is superimposed as a dashed line. In c) and d) the same information is depicted for phen in the presence of an excess of phytate ([phen] = 0.032 mM, [InsP_6] = 0.16 mM).

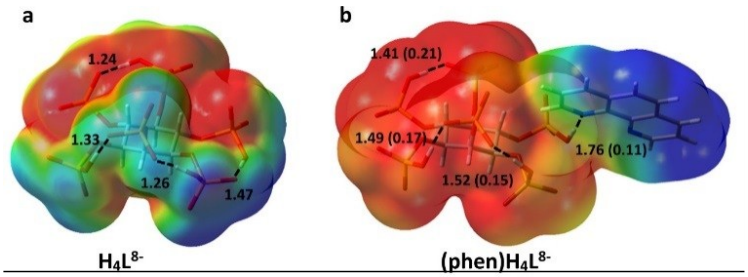

Figure S7. Optimized geometries of H_4L^{8-} (RB3LYP/LANL2DZ) (a) and (phen)H_4L^{8-} (RB3LYP/6-31++G**) (b) species. The electrostatic potential is mapped onto an isodensity surface (isodensity value = 0.0004 e; scale: -0.75 V (red) to -0.66 V (blue) for a, and -0.72 V (red) to -0.40 V (blue) for b)). Intramolecular hydrogen bonds are shown as dashed lines, with the associated distances in Å. The Wiberg bond orders are listed between brackets. Color code: C (grey), H (white), O (red), P (orange), N (blue).

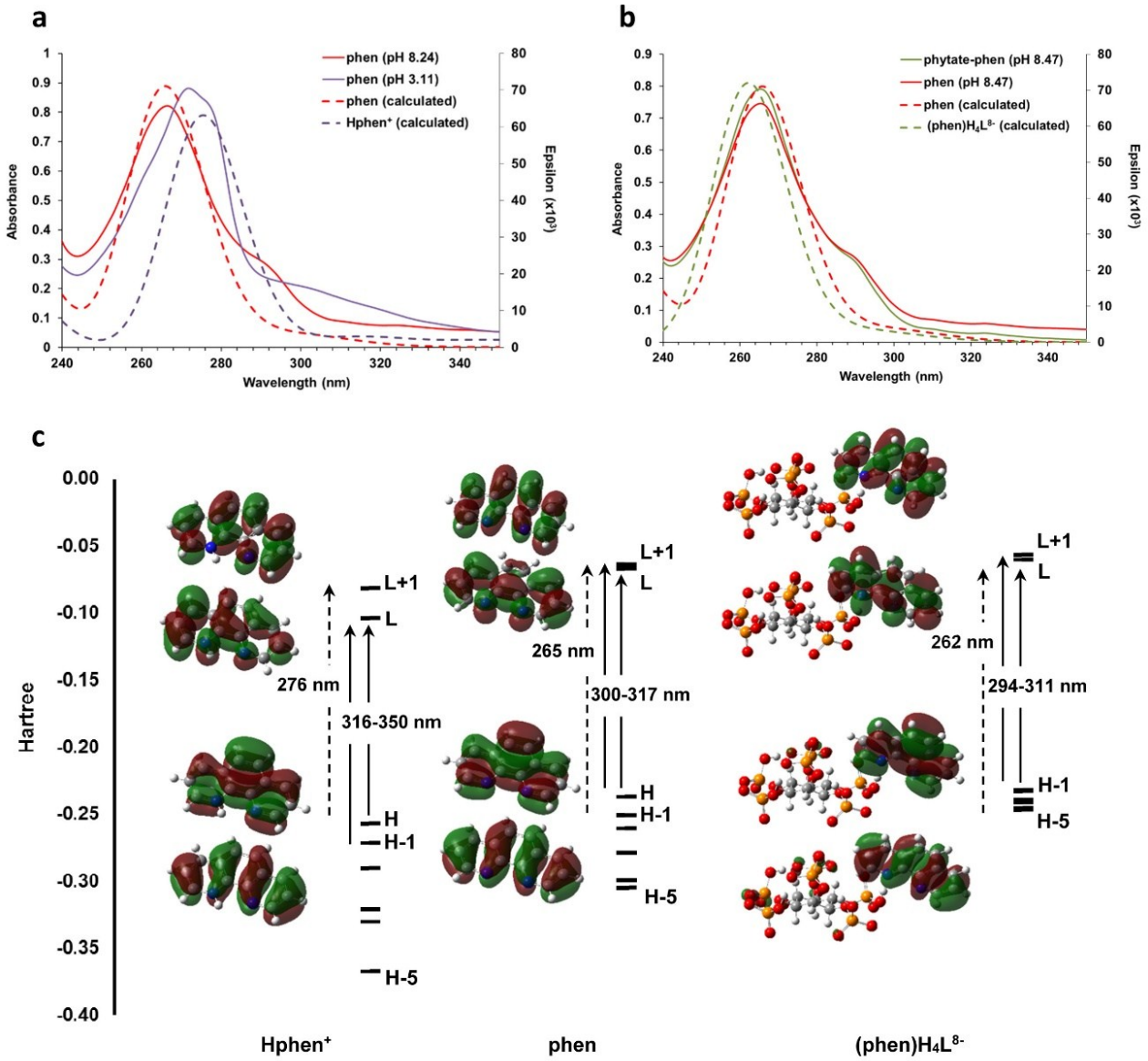

Figure S8 UV-vis spectra of phen (a) and phytate-phen (b) systems. Experimental and calculated spectra for $Hphen^{+}$, phen and $(phen)H_4L^{8-}$ species are depicted as solid and dashed lines, respectively. For the theoretical spectra, the half-width at half height is 0.2 eV. In (c), the molecular orbitals involved in the different electronic transitions and their energy are shown (H = HOMO; L = LUMO). Color code: C (grey), H (white), O (red), P (orange), N (blue).

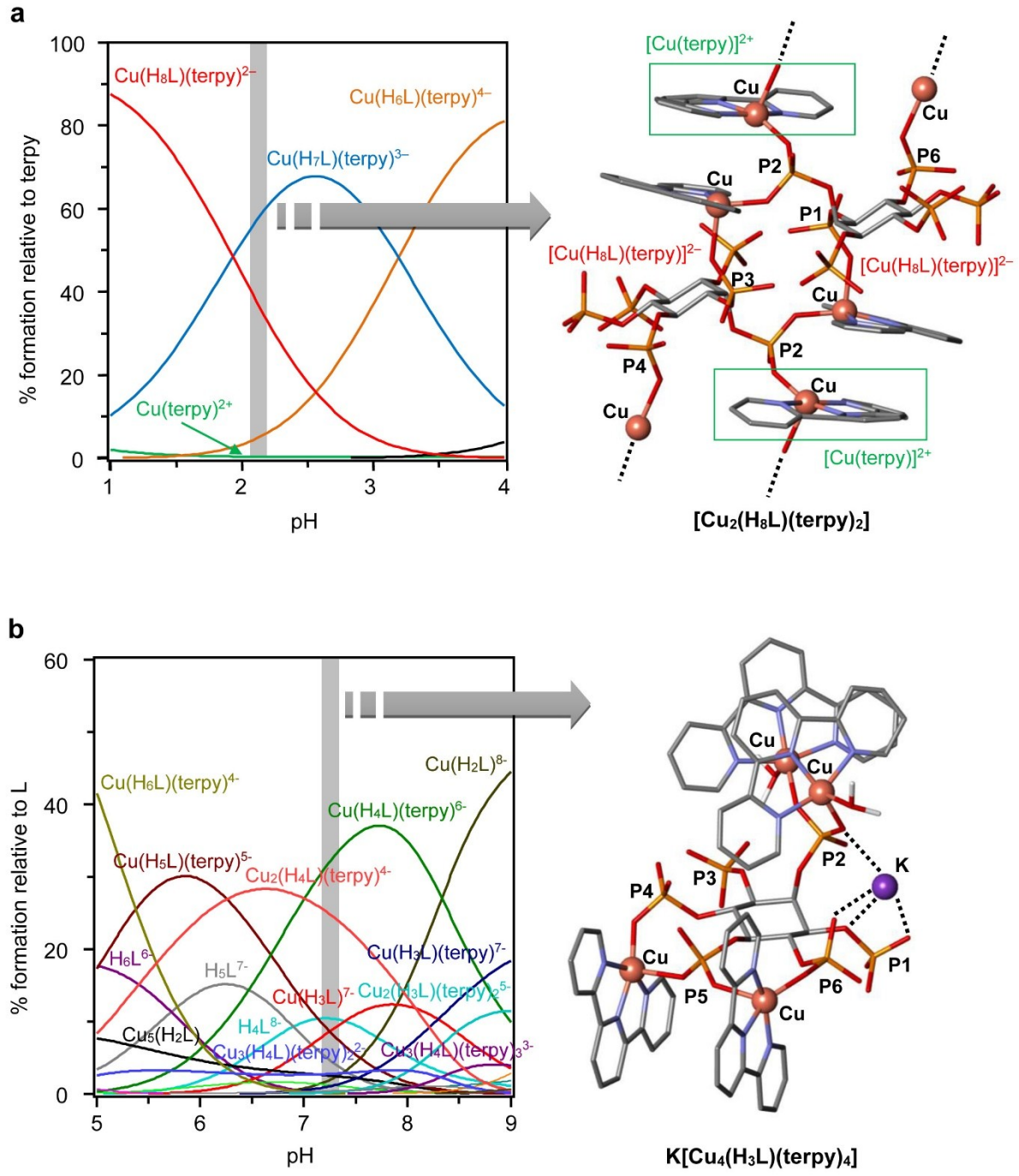

Figure S9. Species distribution under the conditions that led to the formation of compounds $[Cu_2(H_8L)(terpy)_2]\cdot 7.5H_2O$ (a) and $K[Cu_4(H_3L)(terpy)_4]\cdot 26H_2O$ (b) [11]. a) [terpy] = 5.3 mM, [InsP_6] = 7.1 mM, [Cu^{2+}] = 8.2 mM; b) [terpy] = 7.0 mM, [InsP_6] = 9.5 mM; [Cu^{2+}] = 12 mM. Predictions are for 0.15 M NMe_4Cl at 37.0 °C. The pH of the synthesis is highlighted in each case. Color code: C (grey), H (white), O (red), N (blue), P (orange), Cu (pink), K (violet). Some of the hydrogen atoms are omitted for clarity.

References

1 A. W. Coats and J. P. Redfern, *Nature*, 1964, **201**, 68-69.

2 H. H. Horowitz and G. Metzger, *Anal. Chem.*, 1963, **35**, 1464-1468.

3 M. S. Refat, S. A. El-Korashy and A. S. Ahmed, *Spectrochimica Acta Part A: Molecular and Biomolecular Spectroscopy*, 2008, **71**, 1084-1094.

4 L. S. Prabhumirashi and J. K. Khoje, *Thermochim. Acta*, 2002, **383**, 109-118.

5 L. S. Prabhumirashi and J. K. Khoje, *Indian J. Chem. , Sect A*, 2004, **43A**, 299-302.

6 A. L. M. Daneluti and J. Matos, *Brazilian Journal of Pharmaceutical Sciences*, 2013, **49**, 275-283.

7 H. R. Dholariya, K. S. Patel, J. C. Patel and K. D. Patel, *Spectrochimica Acta Part A: Molecular and Biomolecular Spectroscopy*, 2013, **108**, 319-328.

8 G. J. Kharadi, *J Therm Anal Calorim*, 2012, **107**, 651-659.

9 A. Khawam and D. R. Flanagan, *The Journal of Physical Chemistry B*, 2006, **110**, 17315-17328.

10 V. Šáatava, *Thermochim. Acta*, 1971, **2**, 423-428.

11 N. Veiga, J. Torres, C. Bazzicalupi, A. Bianchi and C. Kremer, *Chem. Commun.*, 2014, **50**, 14971-14974.